Effect of writing beam spatial coherence on fiber Bragg grating modulation contrast and thermal stability

Lingyun Xiong* and Jacques Albert

Department of Electronics, Carleton University, 1125 Colonel By Drive, Ottawa, Ontario K1S 5B6, Canada
**Corresponding author: lxiong@doe.carleton.ca*

Received July 17, 2009; revised September 8, 2009; accepted September 14, 2009;
posted September 21, 2009 (Doc. ID 114372); published October 26, 2009

We present a method to fabricate fiber Bragg gratings with adjustable refractive index contrast by using the standard phase mask technique. A theoretical analysis of the diffracted field from the phase mask is performed by considering the effect of the spatial coherence of the incident UV beam. The numerical results show that the grating index contrast decreases as the separation between the fiber and the phase mask increases. Strong gratings with various index contrasts have been inscribed in hydrogen-loaded single mode fibers at different writing distances, and the measured index contrast values are in good agreement with the simulation results. Furthermore, thermal decay tests on the gratings demonstrate that the thermal stability of the grating reflectivity is improved for those gratings fabricated at larger separations between the fiber and the phase mask. These results suggest a one-step process to fabricate gratings with an enhanced thermal stability.

OCIS codes: 030.1640, 060.3735, 060.3738, 120.6780, 120.6810.

1. INTRODUCTION

Fiber Bragg gratings (FBGs) have been widely used for numerous applications in optical communication and fiber optic systems, because they demonstrate ideal characteristics such as cost effectiveness, low insertion loss, compact in-fiber geometry, and flexibility to achieve many desired spectral profiles. Most applications require extremely high tolerances on the optical properties of the grating over long times, and this is dependent on the thermal stability of the UV-induced refractive index change in the grating. The thermal decay curves of gratings are dependent on factors such as fiber composition (core and cladding dopants) and whether hydrogen was used to enhance the photosensitivity, as well as on the grating writing conditions [1–6]. However in all cases the grating decay in silica fibers demonstrates a similar trend, which starts with a fast decay followed by a substantially slower decay as time progresses. It is also well established that weak gratings decay more (in relative terms) than strong gratings. Given these features, a popular approach to stabilize the gratings is to use an accelerated aging process [1]. This process involves annealing gratings at a high temperature to remove the most unstable part of the grating strength (index modulation amplitude): the accelerated aging brings gratings "rapidly" to the state where the decay rate becomes very slow at operating temperatures. Properly annealed gratings will not experience further thermal decay at their expected operational temperature (usually $<75°C$) over a predetermined lifetime (typically 15–25 yr). The need for accelerated aging means that gratings have to be fabricated with up to 30% more index modulation amplitude than the required value because that is how much index strength is removed by the preannealing. To reduce the amount of preannealing required, in other words to fabricate gratings that are inherently more stable to begin with, an alternative approach utilizing pre-exposure or postexposure techniques has been found to be effective in improving the initial grating thermal stability, without involving a heating process [7–9]. This approach includes an additional blanket (uniform) exposure of the UV light either before or after grating inscription. The increased average component of the UV-induced refractive index change (referred to as the "DC" component in the remainder of the text), which is formed during this process has been shown to reduce the thermal degradation of the UV-induced refractive index modulation (the "AC" component of index change), and hence to increase the thermal stability of the grating reflectivity. Although pre-exposure or postexposure techniques can enhance the stability of grating reflectivity, these techniques involve a two-step process, which makes the fabrication of gratings more complex.

We propose instead (experimentally and theoretically) a one-step procedure to inscribe gratings with low index contrast (i.e., with an elevated DC refractive index change) and show that their thermal stability increases with decreasing index contrast [10]. The method is based on a variation of the standard phase mask technique for grating fabrication that takes advantage of the limited spatial coherence of the excimer laser UV beam that we use. The fringe contrast of the interference pattern generated by the phase mask is decreased to any desired level by increasing the distance between the fiber and the phase mask. In the following, a theoretical analysis of the diffracted field distribution behind the phase mask will be performed by taking into consideration the effect of spa-

tial coherence. Previous studies of the diffracted field from the phase mask have been carried out using either an approximate multiple beam interference model or a rigorous coupled-wave model [11–13], but the incident beam was assumed to have ideal spatial coherence in these studies. This assumption is typically valid if the optical fiber is placed close to the phase mask where the diffraction orders are highly coherent with each other. However, the spatial coherence of the incident beam becomes important in the fringe patterns generated by the phase mask if the separation of the fiber from the phase mask increases as we will show here. The only theoretical analysis including the effect of spatial coherence was done by Dyer *et al.* [14], in which the spatial coherence of the incident beam has been taken into account implicitly by including the effect of the angular beam divergence. In comparison, we will explicitly express the spatial coherence by using the fact that the spatial coherence of the excimer laser is governed by the Gaussian–Schell model [15,16]. The simulation results reveal that the grating index contrast is gradually lost as the fiber to phase mask distance increases, and they are in good agreement with the measured index modulation contrast values that we get from fabricated gratings. Furthermore, we report thermal annealing experiments of gratings written at different distances from the phase mask and confirm that the thermal stability of the grating reflectivity is enhanced for those gratings fabricated at larger writing distances.

2. EXPERIMENTAL RESULTS AND THEORETICAL ANALYSIS

A. Grating Fabrication

Figure 1 illustrates our FBG fabrication system. Bragg gratings were written in hydrogen-loaded standard telecommunication fibers (SMF-28 from Corning) by irradiation from a pulsed excimer laser (PulseMaster 840 series from GSI Lumonics). Operating at 248 nm with a gas mixture of KrF, the laser delivered pulses of about 20 ns at a repetition rate of 40 Hz. A combination of apertures and a beam expander with a magnification factor of 2× along the fiber axis direction is used to image the central part of the laser beam uniformly on the fiber samples. The incorporation of the beam expander also increases the spatial coherence length by increasing the distance between two mutually coherent points in the laser beam cross section, but it reduces the pulse energy density of the laser beam. The fluence per pulse incident on the fiber was finally increased to ~189 mJ/cm^2 by using a cylindrical lens to focus the UV light on the fiber axis. A phase mask with a period of 1067.2 nm was placed just in front of the fiber to form a light interference pattern mainly with the +1st and −1st order diffraction beams. As an important parameter of the grating writing condition, the separation between the fiber and the phase mask can be precisely controlled with an accuracy of 10 μm by placing the hydrogen-loaded fiber on a precise translation stage. Before the fabrication of gratings, the optical fibers had been saturated with hydrogen by placing them in a hydrogen filled tube at room temperature and a pressure of ~17.24 MPa (2500 psi) for 14 days. Once gratings were recorded in the hydrogen-loaded fibers, a quick annealing procedure was carried out on these gratings by heating them with a heat gun, in order to remove the most unstable part of the UV-induced index change. This procedure lasts for about 1 min at a temperature in the range of 200°C–400°C, and was monitored to result in a grating erasure of 30% of the as-written grating index modulation amplitude (Erdogan *et al.* state that the combination of heat and duration used to erase a fraction of the index modulation does not matter for the accelerated aging [1]). Following that quick anneal, the residual hydrogen was diffused out by leaving fibers in an oven at 120°C for approximately 12 h.

As the evolutions of the grating transmission spectra have been monitored and recorded continually in the course of the grating inscription, it is possible to show the evolution of both DC and AC components of the UV-induced refractive index change in the grating. More specifically, the mean refractive index change Δn_{mean} is derived from the Bragg wavelength shift during the grating inscription, and the modulation amplitude of the refractive index change Δn_{mod} is calculated from the grating transmission notch depth using the standard expressions for uniform gratings [17] (as mentioned before our irradiation pattern is highly uniform because we use only a small fraction of the expanded laser beam). As the UV-induced refractive index change is assumed to exist only inside the fiber core, the calculations of both Δn_{mean} and Δn_{mod} have taken the power confinement factor (0.75) of the code mode into consideration. It has to be mentioned

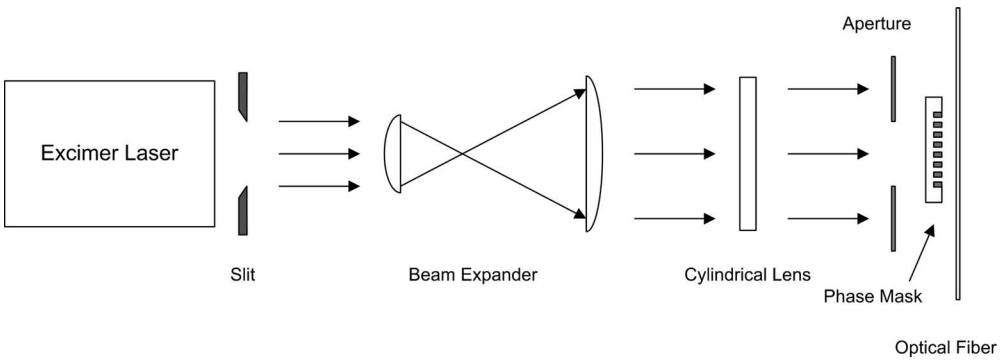

Fig. 1. Schematic of FBG fabrication system.

that the mean refractive index change Δn_{mean} represents the absolute change in the fiber core index instead of the change in the mode effective index.

Figure 2 shows the grating growth behavior during the formation of 3 mm long hydrogen-loaded FBGs. Under identical UV pulse irradiation conditions, three gratings have been written at different distances between the fiber and the phase mask: 100, 600, and 1000 μm. To be precise, by taking the fiber cladding dimension into account, the above writing distances correspond to fiber core to phase mask distances of 162.5, 662.5, and 1062.5 μm. In this figure, both the mean refractive index change Δn_{mean} and the refractive index modulation Δn_{mod} for three gratings are illustrated as functions of the exposure time. It is important to note that, for the calculation of Δn_{mod} in such short gratings, we have to take into consideration the grating modulation length reduction due to the diminishing length of overlap of the two interfering beams (+1 and −1), when the fiber to phase mask distance increases. At a distance of 1062.5 μm, for instance, the length of the interference pattern reduces from 3 to 2.5 mm.

As illustrated in Fig. 2, both the DC and AC components of the refractive index change increase nearly linearly as the exposure time. At the writing distance of 162.5 μm, the growth rate of the refractive index modulation is almost the same as that of the mean refractive index change, which means the formation of a perfect interference fringe pattern. In contrast, substantial decreases in the growth rate of the index modulation are demonstrated as the fiber core to phase mask distance moves up to 662.5 and 1062.5 μm. At 662.5 μm, in order to induce the same Δn_{mod} of $\sim 6.39\times10^{-4}$ as that at 162.5 μm, a longer exposure time is needed, which results in Δn_{mean} of 2.00×10^{-3} formed inside fiber core compared with 5.96×10^{-4} for a distance of 162.5 μm. At 1062.5 μm, we can only induce Δn_{mod} of $\sim 1.42\times10^{-4}$ even with a longer exposure time than at 662.5 μm. Another point of the grating growth behavior observed in the figure is that the mean refractive index change grows at a similar rate for all writing distances.

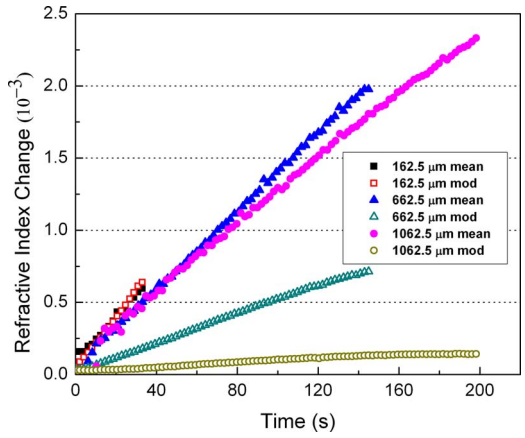

Fig. 2. (Color online) Change in grating UV-induced index change versus the UV exposure time for gratings written at fiber core to phase mask distances of 162.5, 662.5, and 1062.5 μm. The mean refractive index changes of gratings are represented by closed symbols, and the refractive index modulation amplitudes are represented by open symbols.

B. Theoretical Analysis of the Diffraction Field Behind the Phase Mask

Theoretical modeling of the diffraction field distribution behind the phase mask requires the consideration of the effect of the spatial coherence of the incident beam. The interference and diffraction of a partially coherent light source can be calculated by the van Cittert–Zernike theorem [18], which introduces a parameter called the degree of coherence to describe the coherence between two points on the source. For the sake of simplicity, the diffraction field behind the phase mask can be treated as the interference field between the +1st, 0th, and −1st order diffracted plane waves, which are at least partially coherent with each other as a result of the spatial coherence. Hence, the intensity distribution described by the Zernike formula can be simplified as three-beam interference, which takes the following form:

$$I(x,z) = I_1 + I_{-1} + I_0 + 2\sqrt{I_1}\sqrt{I_{-1}}j(P_1,P_{-1})\cos(2k_{x1}x) + 2\sqrt{I_1}\sqrt{I_0}j(P_1,P_0)\cos[k_{x1}x + (k_{z1}-k)z] + 2\sqrt{I_{-1}}\sqrt{I_0}j(P_{-1},P_0)\cos[-k_{x1}x + (k_{z1}-k)z], \quad (1)$$

where I_1, I_{-1}, and I_0 are the intensities of the +1st, −1st, and 0th order diffracted beams; $j(P_1,P_{-1})$, $j(P_1,P_0)$, and $j(P_{-1},P_0)$ are the degrees of coherence between any two of the three diffracted beams; coordinates x and z are the dimensions along the directions tangential and normal to the phase mask surface, respectively; k_{x1} and k_{z1} are the x and z components of the wave vector of the first order diffracted beam; and k is the wave vector of the zeroth order diffracted beam. We assume uniformity of the waves in the y direction.

The spatial coherence of the KrF excimer laser beam can be characterized by the Gaussian–Schell model, which is used in [15,16]. In this model, the degree of coherence $j(x_1,x_2)$ between two points in the cross section of the laser beam is a Gaussian function $j(x_1,x_2)=\exp[-(x_1-x_2)^2/2\sigma_x^2]$, where σ_x is the coherence width of the laser beam. Using the triangle geometry relationship shown in Fig. 3, the coherence functions in Eq. (1) for any point located at a distance z away from the mask is given by

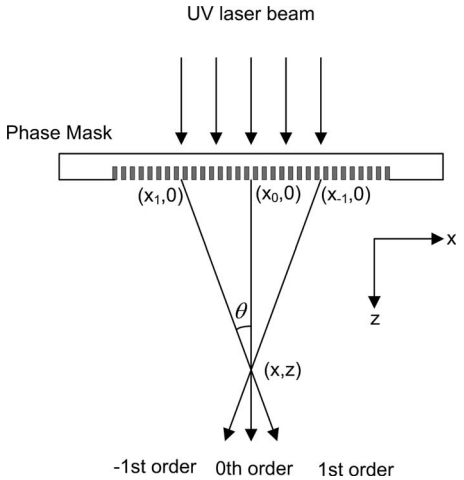

Fig. 3. Geometry of the irradiation, showing the origin of the three beams that interfere at point (x,z) behind the phase mask.

$$j(P_1,P_{-1}) = \exp[-(x_1 - x_{-1})^2/2\sigma_x^2] = \exp[-(2z\ \tan\ \theta)^2/2\sigma_x^2], \tag{2}$$

$$j(P_1,P_0) = j(P_{-1},P_0) = \exp[-(x_1 - x_0)^2/2\sigma_x^2] = \exp[-(z\ \tan\ \theta)^2/2\sigma_x^2], \tag{3}$$

where θ is the diffraction angle of the first order diffracted beams relative to the incident beam direction.

Note that, in the simulation, the intensity distribution of the incident laser beam is assumed to be a uniform instead of a Gaussian distribution, which means that I_1, I_{-1}, and I_0 are constant independent of the coordinate x. This corresponds to our experimental situation because the incorporation of the apertures and beam expander allow us to image the uniform central part of the incident beam on the phase mask.

The intensity distribution of the field behind the phase mask has been investigated by Dyer *et al.* with a numerical analysis in which the spatial coherence of the incident beam has also been included implicitly through the angular beam divergence [14]. Here, we explicitly express the spatial coherence of the classical diffraction theory, with a coherence function that is a Gaussian function according to the well established Gaussian–Schell model [15,16].

In the simulations carried out with Eqs. (1)–(3), the intensities I_1, I_{-1}, and I_0 are normalized to the incident intensity and are hence equal to the diffraction energy efficiencies for the $\pm$1st and 0th orders: 33% and 2%, respectively. Several simulations were carried out with different values of σ_x. The results shown here correspond to a coherence width σ_x of 228.9 μm, which was found to provide the best fit between the simulated index contrasts and the experimental values, which will be described at the end of this section. The computed field intensity distribution behind the phase mask of an incident laser beam with finite coherence is illustrated in Fig. 4. The distributions are computed for a region that covers a few periods in the x direction ($-1.334 \le x \le 1.334$ μm) and a large writing distance in the z direction ($0 \le z \le 1400$ μm). As shown in Fig. 4, the fringe pattern generated by the phase mask is periodically varying along the x direction with the period of $\Lambda/2$, where Λ is the period of the phase mask. In the z direction, the visibility of the interference fringes is gradually lost when the distance from the phase mask increases. The fringe pattern becomes a nearly uniform distribution at the largest writing distance of $z = 1400$ μm. This gradual variation in the z direction is a result of the effect of the finite spatial coherence. One point worth noting is that, due to the existence of some zeroth order diffraction, there is an additional periodical variation along the z direction (the Talbot effect, with a period of $\sim$10 μm here, is too small to observe on the scale of Fig. 4). It turns out, as we show below, that the $\Lambda/2$ periodic pattern in x seen in Fig. 4 is actually obtained by averaging of the Talbot pattern along the z direction.

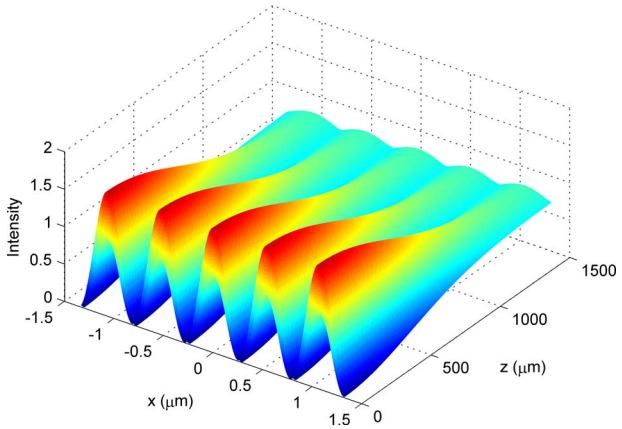

Fig. 4. (Color online) Field intensity distribution behind the phase mask for a partially coherent incident beam with x and z axes parallel and normal to the phase mask surface.

To clearly demonstrate the fringe patterns in both x and z directions, the intensity distributions over a small area of 2.668 μm $\times$ 20 μm are plotted for three different writing distances from the phase mask in Fig. 5, as well as the ideal two-beam interference in the absence of zero order (only from the +1 and $-$1 diffraction orders) for the sake of comparison. With no zero order, a standard sinusoidal fringe pattern with a period of $\Lambda/2$ is clearly seen in Fig. 5(a), and no variation exists along the z direction. When some zero order transmission is included (2% of incident intensity) in the analysis, as shown in Figs. 5(b)–5(d), all of the fringes patterns formed by the phase mask at various writing distances are deviating from ideal sinusoidal fringes, and the field intensity is also periodically changing along the z direction in addition to the typical x-dependent periodical variation. This periodical behavior in the z direction should be attributed to the presence of the zeroth diffraction order, which introduces this variation through the summation of the last two terms in Eq. (1). Inspecting the patterns in Figs. 5(b)–5(d), we can find that the dominant interference peaks are separated by Λ instead of $\Lambda/2$ in the direction of the x coordinate. Hence, the fringe pattern behind the phase mask is not exactly a series of fringes with period of $\Lambda/2$, as we mentioned before, but consists of two systems of Λ fringes alternating in the z direction with a spatial shift of $\Lambda/2$ in the x direction.

However, this fact will not change the Bragg wavelength of the grating inscribed on the single mode fiber. As shown in Figs. 5(b)–5(d), the fiber core with diameter of 8 μm, which is indicated by the solid lines for each writing distance, covers almost a full period in the z direction of the fringe pattern. When averaged over this fiber core diameter along the z direction, the fringes retain most of the characteristics of the two-beam interference patterns with a dominant $\Lambda/2$ fringe period. Comparing the distributions at three distances, we can find that the fringe patterns change in both shape and visibility as the writing distance z increases. The fringe patterns lose contrast at a distance of around $z = 1062.5$ μm as the interfering beams are nearly out of coherence. The change in the shape of the fringe pattern at different writing distances is caused by the altered relative ratio of the mutual intensities of +1st, $-$1st, and 0th diffraction orders, which are represented by the last three terms in Eq. (1).

The normalized AC/DC index contrast of FBGs from both experiment and simulation results are plotted as a function of the distance between the phase mask and the

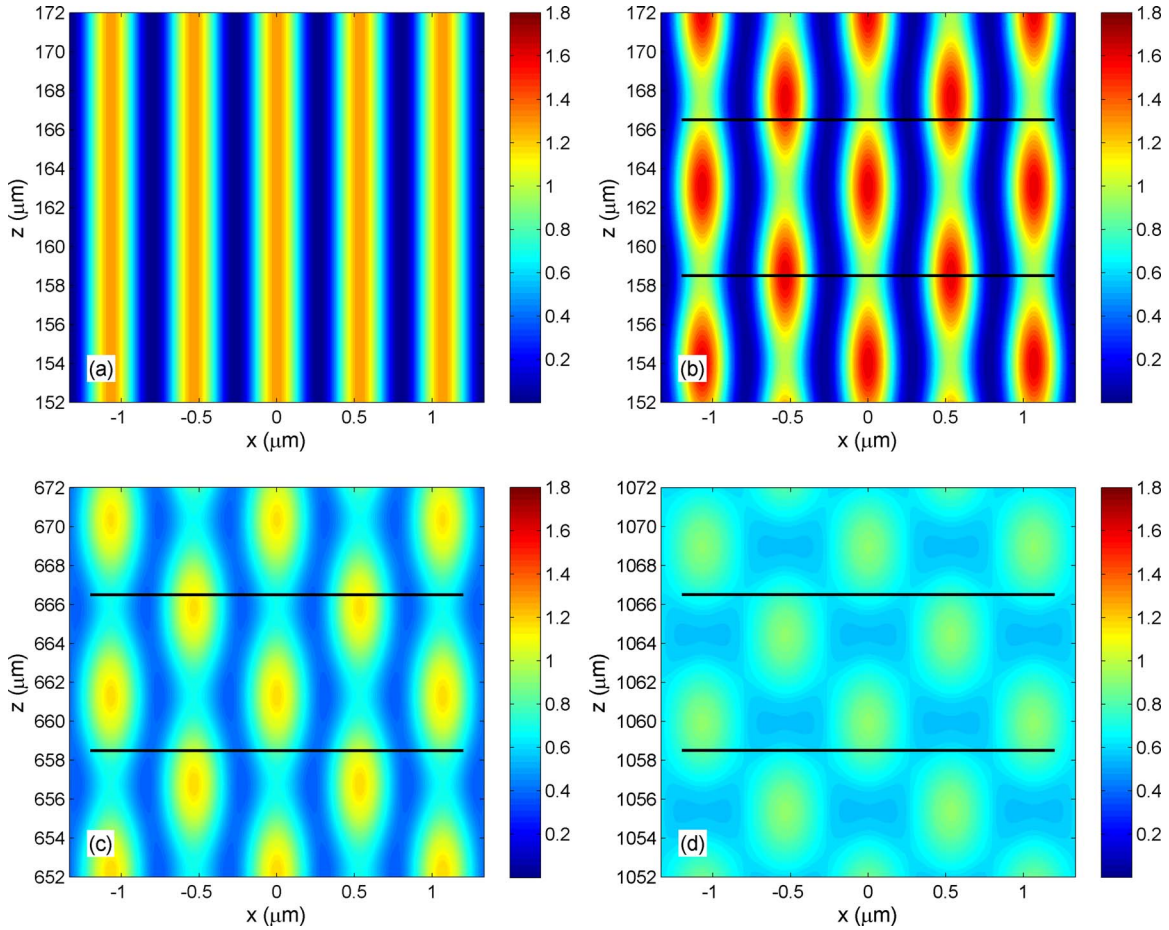

Fig. 5. (Color online) 2D field intensity distribution behind the phase mask at various writing distances from the phase mask: (a) ideal two-beam interference (used for comparison), (b) $z=152-172$ μm, (c) $z=652-672$ μm, and (d) $z=1052-1072$ μm.

fiber core in Fig. 6. Gratings have been fabricated at various writing distances from 162.5 to 1062.5 μm, and the index contrast of each grating in terms of the ratio of the AC index change to the DC index change is calculated and plotted as a single diamond in the figure. The simulated index contrast is obtained from the simulated fringe visibility after the fringes have been averaged over the dimension of the fiber core in the z direction. This calculation is carried out for several values of coherence width σ_x until the theoretical curve fits the experimental points: the best fit is obtained for $\sigma_x=228.9$ μm. As illustrated in the figure, the fitted numerical simulation is in good agreement with the experimental results, and this confirms the validity of the Gaussian–Schell model [15,16] for our situation. The distance along z for which the interference pattern loses contrast is determined by the combination of the angle of the interfering beams and the value of σ_x. While the former quantity depends on the writing laser wavelength and period of the phase mask, the latter is an inherent property of the writing laser beam incident on the mask.

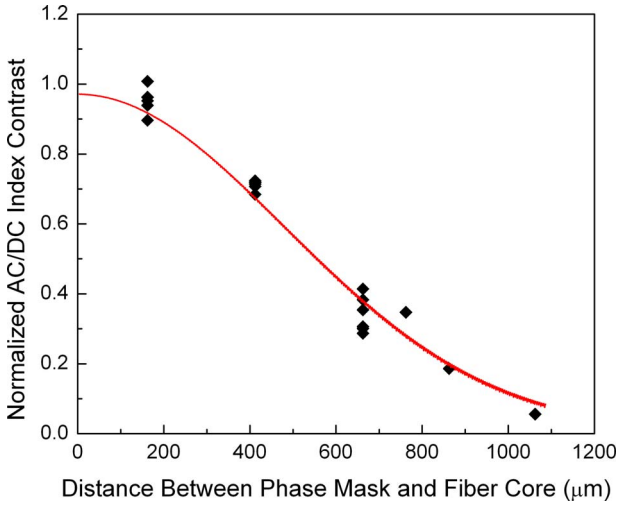

Fig. 6. (Color online) Experimental FBG index contrast as a function of the distance between the phase mask and the fiber core (diamonds). The simulation (curve) is fitted to the experimental data by optimizing σ_x.

C. Thermal Annealing Experiment on Gratings

The impact of the distance between the phase mask and the fiber core (i.e., grating index contrast) on the thermal stability of grating reflectivity has been investigated by using an isothermal annealing process. Gratings with nearly identical index modulations ($\sim 6.5\times10^{-4}\pm0.3\times10^{-4}$ as written and all preannealed by 30%) fabricated at different fiber core to phase mask distances (162.5, 412.5, and 662.5 μm) were annealed at various temperatures. The experimental data were accumulated by mea-

suring the transmission spectra of all gratings every 60 s, and gratings were held at their annealing temperatures (200°C, 250°C, and 300°C) for durations that were sufficiently long (typically several weeks) to yield observable clear thermal decay characteristics. The thermal decays of the grating strength as a function of the annealing time are illustrated in Fig. 7. In the figure, the grating strength is represented by a quantity η called the normalized integrated coupling constant (NICC), a quantity that is proportional to the index modulation amplitude and that is normalized to the initial value prior to the thermal annealing. Each thermal decay curve is the averaged data of two nominally identical gratings, which are fabricated at the same writing distance and annealed at the same temperature. The error bars represent the standard deviation of the decay curves of both gratings from the average curve. Note that all of these hydrogen-loaded FBGs have been preannealed (removal of about 30% of the index modulation) prior to the start of the isothermal annealing, as mentioned before.

When the thermal decay is plotted with linear vertical and horizontal (time) scales, as in the inset of Fig. 7(a), each grating exhibits an initial sharp decrease in the NICC, followed by a progressively slower decay but with a nonzero rate of change. This feature of thermal decay is fundamental to the practice of stabilizing grating structures by accelerated aging, which is generally carried out as heating gratings at higher temperature to force them to reach the slow decay region. To clearly display and compare the thermal decay of gratings, the thermal degradations of gratings are alternately presented with respect to the logarithmic scale of time as shown in Figs. 7(a)–7(c). The main finding is that the thermal stability of gratings fabricated at 662.5 μm is substantially stronger than that of gratings fabricated at shorter writing distances. For the gratings at 412.5 and 162.5 μm, the differences observed fall within the range of experimental error and there is no clear stability difference. Unfortunately, it was not possible to write gratings with the same refractive index modulation at 1062.5 μm because of the loss of coherence, thereby preventing the realization of a fully comparable thermal stability study for that case.

The results shown here demonstrate that the thermal stability of the refractive index modulation Δn_{mod} in a hydrogen-loaded FBG can be improved by increasing the fiber core to phase mask distance past a point where the fringe visibility drops below approximately 0.4. The increment of the average index change obtained by increasing the writing distance from 162.5 to 412.5 μm, which corresponds to the AC/DC index contrast decreasing from 0.9175 to 0.6739, is not large enough to enhance the thermal stability of the index modulation. Only when the AC/DC index contrast decreases to 0.3752 at a distance of 662.5 μm does a substantial improvement of the thermal

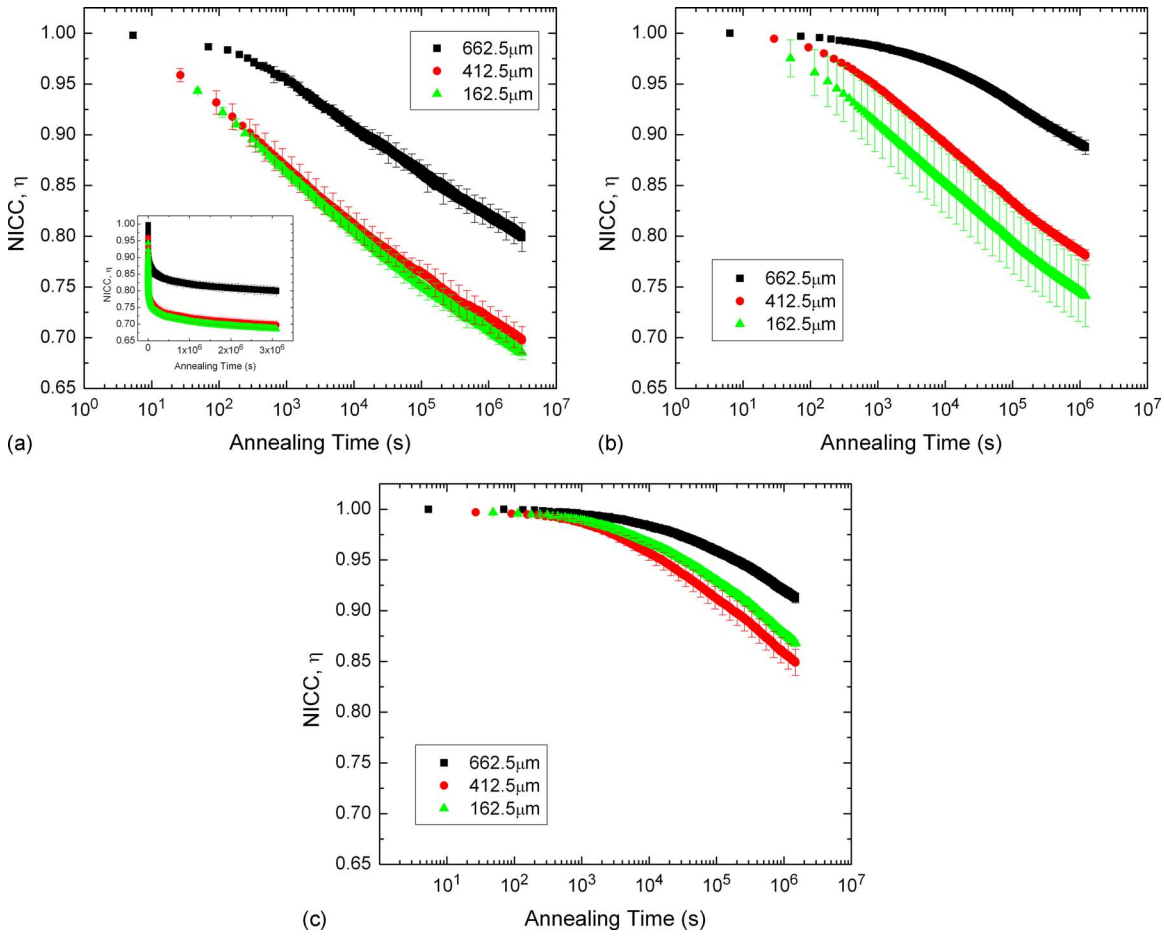

Fig. 7. (Color online) Thermal decay of gratings as a function of annealing time at temperatures of (a) 300°C (the inset shows the thermal decay curves with a linear time scale), (b) 250°C, (c) 200°C.

stability occur. We believe that a further stability improvement can be obtained if we fabricate gratings at larger separation between the phase mask and the fiber core (such as 1062.5 μm). However, as a result of the poor fringe visibility at such a long writing distance, the maximum achievable grating refractive index modulation is reduced and may not be sufficient to realize certain types of high reflectivity fiber gratings.

Our experiments confirm the general conclusion that an improvement in the thermal stability of grating reflectivity occurs in gratings with a large uniform index change superimposed on the refractive index modulation amplitude that gives rise to the reflection properties of the grating, as noted for nonhydrogenated FBG in [8], where the grating average index change is increased by the postfabrication of a uniform UV exposure on the grating, and for a pre-exposed grating in hydrogenated fiber [9].

3. CONCLUSION

In conclusion, we have fabricated Bragg gratings with various index contrasts in hydrogen-loaded single mode fibers using a simple variation in the standard phase mask technique. Low index contrasts are achieved at a large separation between the phase mask and the fiber as a result of the limited spatial coherence of the incident beam. A theoretical analysis of the diffracted field from the phase mask has been performed, including the contribution of the spatial coherence of the excimer laser, as modeled by a Gaussian–Schell representation [15,16]. The numerical results demonstrate that the grating index contrast is gradually lost as the writing distance increases, with a functional shape that agrees with the experimentally measured index contrast values of fabricated grating samples. Further thermal decay tests on the gratings show that the thermal stability of the grating reflectivity for gratings fabricated at writing distances large enough to decrease the index contrast below 0.4 is stronger than that for gratings fabricated at shorter writing distances. Therefore, this simple one-step grating fabrication procedure can be used to inscribe gratings with low index contrast and enhanced grating thermal stability. For volume production, the use of a phase mask with some zero order transmission would achieve the same result very reproducibly. A corollary conclusion further indicates that the precise control of the distance between the fiber and the phase mask does not appear to have a measurable impact within a range of about 100–200 μm, thereby relaxing manufacturing tolerances and increasing the reliability of the writing process by positioning the fiber far enough from the mask to prevent accidental contact.

ACKNOWLEDGEMENTS

The financial support from the Natural Sciences and Engineering Research Council (NSERC) of Canada is gratefully acknowledged. J. Albert is further supported by the Canada Research Chairs program.

REFERENCES

1. T. Erdogan, V. Mizrahi, P. J. Lemaire, and D. Monroe, "Decay of ultraviolet-induced fiber Bragg gratings," J. Appl. Phys. **76**, 73–80 (1994).
2. S. Kannan, J. Guo, and P. J. Lemaire, "Thermal stability analysis of UV-induced fiber Bragg gratings," J. Lightwave Technol. **15**, 1478–1483 (1997).
3. S. Baker, H. Rourke, V. Baker, and D. Goodchild, "Thermal decay of fiber Bragg gratings written in boron and germanium codoped silica fiber," J. Lightwave Technol. **15**, 1470–1477 (1997).
4. S. Ishikawa, A. Inoue, M. Harumoto, T. Enomoto, and H. Kanamori, "Adequate aging condition for fiber Bragg grating based on simple power low model," in *Proceedings of the OFC* (1998), pp. 183–184.
5. J. Rathje, M. Kristensen, and J. E. Pederson, "Continuous anneal method for characterizing the thermal stability of ultraviolet Bragg gratings," J. Appl. Phys. **88**, 1050–1055 (2000).
6. N. K. Viswanathan and D. L. LaBrake, "Accelerated-aging studies of chirped Bragg gratings written in deuterium-loaded germano-silicate fibers," J. Lightwave Technol. **22**, 1990–2000 (2004).
7. E. Salik, D. S. Starodubov, V. Grubsky, and J. Feinberg, "Thermally stable gratings in optical fibers without temperature annealing," in *Proceedings of the OFC* (1999), pp. 56–58.
8. Q. Wang, A. Hidayat, P. Niay, and M. Douay, "Influence of blanket postexposure on the thermal stability of the spectral characteristics of gratings written in a telecommunication fiber using light at 193 nm," J. Lightwave Technol. **18**, 1078–1083 (2000).
9. M. Aslund and J. Canning, "Annealing properties of gratings written into UV-presensitized hydrogen-outdiffused optical fiber," Opt. Lett. **25**, 692–694 (2000).
10. L. Xiong and J. Albert, "Thermal stability of excimer laser-written fiber Bragg gratings as a function of fiber/phase mask distance," Proc. SPIE **6796**, 67961B (2007).
11. J. Mills, C. J. Hillman, B. Blott, and W. Brocklesby, "Imaging of free-space interference patterns used to manufacture fiber Bragg gratings," Appl. Opt. **39**, 6128–6135 (2000).
12. D. Park and M. Kim, "Simple analysis of the energy density distribution of the diffracted ultraviolet beam from a fiber Bragg grating phase mask," Opt. Lett. **29**, 1849–1851 (2004).
13. Z. Hegedus, "Contact printing of Bragg gratings in optical fibers: rigorous diffraction analysis," Appl. Opt. **36**, 247–252 (1997).
14. P. E. Dyer, R. J. Farley, and R. Giedl, "Analysis of grating formation with excimer laser irradiated phase masks," Opt. Commun. **115**, 327–334 (1995).
15. T. Kajava, A. Hakola, H. Elfstrom, J. Simonen, P. Paakkonen, and J. Turunen, "Flat-top profile of an excimer-laser beam generated using beam-splitter gratings," Opt. Commun. **268**, 289–293 (2006).
16. Y. Cai and S. He, "Partially coherent flattened Gaussian beam and its paraxial propagation properties," J. Opt. Soc. Am. A **23**, 2623–2628 (2006).
17. A. Othonos and K. Kalli, *Fiber Bragg Gratings: Fundamentals and Applications in Telecommunications and Sensing* (Artech House, 1999).
18. M. Born and E. Wolf, *Principles of Optics* (Cambridge U. Press, 1999).